博士論文（要約）

Doctorate Thesis

Interplay between geometrical and electronic structure within the two dimensional surface lattice probed by iron phthalocyanine

（鉄フタロシアニン表面二次元格子中の構造と電子状態の相関）

Department of Advanced Materials Science
Graduate School of Frontier Sciences
The University of Tokyo

Naoka Ohta

東京大学大学院 新領域創成科学研究科 物質系専攻

太田 奈緒香

Thesis

Interplay between geometrical and electronic structure within the two dimensional surface lattice probed by iron phthalocyanine

鉄フタロシアニン表面二次元格子中の構造と電子状態の相関

A Thesis Submitted to the University of Tokyo
for the Degree of Doctor of Science

By Naoka Ohta

Department of Advanced Materials Science
Graduate School of Frontier Sciences
The University of Tokyo

February, 2015

Supervised by Professor Maki Kawai

Table of contents

Abbreviations

DFT density functional theory

FePc iron phthalocyanine

FIM Field ion microscope

FWHM full width at half maximum

GMR giant magneto resistance

HDD hard disk drive

HREELS high resolution electron energy loss spectroscopy

IETS inelastic electron tunneling spectroscopy

IR infrared

LEED low electron energy diffraction

MBE molecular beam epitaxy

NRG numerical renormalization group

PES photo electron spectroscopy

RKKY interaction Ruderman-Kittel-Kasuya-Yosida interaction

SAM self-assembled monolayer

STM scanning tunneling microscope/microscopy

STS scanning tunneling spectroscopy

TMR tunnel magneto resistance

UHV ultrahigh vacuum

VTI variable temperature insert

XAS x-ray absorption spectroscopy

Symbols

I tunneling current

V_s sample bias voltage

Physical Constants

The values are 2010 CODATA recommended values.* The numbers in the parenthesis are uncertainty of the last two digits.

Planck constant $h = 6.62606957(29) \times 10^{-34}$ J・s = $4.135667516(91) \times 10^{-15}$ eV・s

Planck constant over 2π $\hbar = h/2\pi$

Elementary charge $e = 1.602176565(35) \times 10^{-19}$ C

Electron mass $m_e = 9.10938291(40) \times 10^{-31}$ kg

Bohr magneton $\mu_B = 9.27400968(20) \times 10^{-24}$ J/T = $5.7883818066(38) \times 10^{-5}$ eV/T

Boltzmann constant $k_B = 1.3806488(13) \times 10^{-23}$ J/K = $8.6173324(78) \times 10^{-5}$ eV/K

*http://physics.nist.gov/cuu/Constants/Table/allascii.txt (view:20141217)

Chapter 1

Introduction

1.1 Preface

In this thesis, the author purposed to evaluate influences of the molecule-substrate interaction and the molecule-molecule interaction on the electronic and the spin state of a molecule adsorbed on a metal substrate. Functionalizing molecules and integrating them are proposed to be an ultimate method to miniaturize electronic devices [1]. Elements of electronic devices are supported by a substrate. A molecule supported by a substrate interacts with the substrate through charge transfer, hybridization, magnetic interaction *etc.* These interactions are expected to modify the valence number, the electronic configuration and the spin state of the molecule. For example, antiferromagnetic interaction between the molecular spin and the conduction electrons lead to Kondo screening of the molecular spin [2]. Hybridization and magnetic interaction also occur between molecules. These interactions are expected to make the electronic and the spin state of the molecule which interact with the other molecules different from those of isolated molecule. Conversely, intermolecular interaction can be evaluated by comparing the electronic and the spin state of molecules in different environment (isolated, making dimer, trimer, cluster..). This is accomplished by measuring the electronic and the geometric structure of a molecule simultaneously. Scanning tunneling microscope (STM) suits for the measurement since it works as both microscope and spectroscope. In this thesis, we examined the influence of molecule-substrate and molecule-molecule interaction on the electronic and the spin state of a molecule adsorbed on metal substrates mainly by using STM.

In this chapter, we describe the background and the objective of the study. First, we introduce the tendency of refinement of elements of electronic devices. We introduce that self-assembly of functional molecules is considered as the ultimate method for refinement. Next, we introduce magnetism of iron phthalocyanine

(FePc). Magnetic molecules are typical functional molecules. FePc is one of the magnetic molecules, and considered as an archetypal functional molecule. Recently, magnetism of individual FePc adsorbed on substrates has been investigated using STM. Magnetic properties of bulk FePc and those of FePc on substrates is reviewed briefly. Recent understanding on effect of molecule-substrate interaction on the spin state of FePc is summarized. Finally, we describe our objective of the study. In this study, we utilized self-assembly of FePc to detect inter molecular interaction. We employed Ag(111), Ag(110), Ag(100) and Au(111) as the substrate. The reason why we chose these substrates and the purpose of the study is summarized. In chapter 2, we introduce the apparatus and methods we used for the study. As measurement technique, we used high resolution electron energy loss spectroscopy (HREELS) in addition to STM. Mechanism of STM for microscopy and spectroscopy (Scanning tunneling spectroscopy, STS), mechanism of HREELS, and the ultrahigh vacuum systems used for the study are introduced. The method of sample preparation is also described. In chapter 3, we describe spin and vibration excitations of FePc adsorbed on Ag(111), Ag(110) and Ag(100) surface. We show dependence of the STS spectra on the geometrical configuration. We discuss effect of the local environment of the molecules on the electronic structure of the molecule. In chapter 4, we introduce our investigation on the collective magnetic state of FePc forming lattice on Au(111). Spatial distribution of the STS spectra and its dependence on the external magnetic field is described. We show that an Ising type antiferromagnetic ordering of the system well explain the results. Chapter 5 is the summary of the study.

1.2 Background

1.2.1 Tendency of refining of elements in electronic devices

The elements in electronic devices are becoming smaller in recent decades. The widths of the wires in large-scale integrated circuits and magnetic memories in hard disk drive (HDD) are now smaller than tens of a few nanometers [3,4]. The advances have been propelled by appearance of new techniques. For example, development of molecular epitaxy (MBE) in 1970's has played important role in raising degree of integration of magnetic memories [5]. In 1987, Fert and Grünberg created Fe-Cr-Fe super lattice using MBE and discovered that it shows giant magneto resistance [6,7]. The resistivity of the thin layer of chromium changes drastically depending on the relative direction of the magnetization of the two iron layers which sandwich the chromium layer. The discovery was applied for read head of HDD, which has accelerated miniaturization of the read head and the magnetic memories. Fert and Grünberg were awarded Nobel Prize in Physics for the discovery in 2007.

Use of molecular devices and integration of them have possibility to contribute to further refinement of the electronic devices. It has been proposed that by controlling the functionality of a molecule using chemical technique, the molecule work as an elemental device [1]. Magnetic molecules have been considered as a prototype of functional molecules. Thus, the properties of individual magnetic molecules adsorbed on substrates are of interest. We introduce in the following text that studies using STM has been contributed to reveal the magnetism of individual molecules adsorbed on metal substrates.

1.2.2 Studies on magnetism of molecules using STM

STM is a powerful tool to measure the geometric and the electronic structure of a surface simultaneously. It was invented by Binnig, Rohrer, Gerber and Weibel in 1982 [8,9]. Binnig and Rohrer were awarded Nobel Prize in Physics for the invention in 1986. Using STM, we can obtain real space image of the sample surface with atomic resolution [10]. We can also conduct spectroscopy, STS, using STM. Local electronic density of states [11], spin excitation energies [12] and vibrational excitation energies [13] were measured using STS. (The mechanism of the STM and STS is introduced in chapter 2.) The energy resolution of STS is mainly determined by the temperature of the sample ~5.4 $k_B T$ [14], and can be made better than 1 meV by using commercially available equipment. The high energy resolution allows us to resolve fine structures related to the spin degrees of freedom including spin excitations [12,15-25], Kondo resonance [12,17,18,26-30] and their response to external magnetic fields. The concentrated nature of the tunneling current also allows us to resolve inhomogeneity of the sample.

FePc is one of the magnetic molecules. Effects of molecule-substrate interaction on the spin state of the FePc adsorbed on substrates is studied by using STM and other methods [19,28,29]. According to the studies, the spin state of FePc is different from those of FePc in bulk. Molecular structure of FePc in bulk is shown in Fig. 1.1. The molecule has D_{4h} symmetry and planer cross shaped configuration [31]. Two types of polymorphs are reported for single crystal of FePc: α type [32] and β type [33]. Both polymorphs are so called “herring bone” type; the molecules arrange in the column extending along the direction of b axis of the crystal, tilting the four fold axis from the b axis to opposite direction in adjacent columns. The tilt angle is different for the α and β polymorphs as schematically shown in Fig. 1.2. In both polymorphs, the spin state of FePc is considered to be S=1 [34,35]. As the temperature decreases the α polymorphs of FePc becomes ferromagnetic below 10 K [35] while the β polymorphs of FePc remains being paramagnetic even at 1.25 K [34,36]. Reflecting the anisotropic geometry of the crystal, the magnetic interaction intra and inter molecular column of the α polymorphs of FePc is reported to be ferromagnetic and weak antiferromagnetic respectively [35]. Spin states of FePc adsorbed on Cu(110) [19], oxidized Cu(110) (Cu(110))2×1))-O) [19] and Au(111) [28,29] substrate have been studied using STM, photoelectron spectroscopy (PES) and density functional theory (DFT) calculations. It was proved by using PES that the spin state of FePc adsorbed on the bare Cu(110) surface changes from S=1 to S=0 [19]. In contrast, it was shown by STM and PES that the spin state of FePc adsorbed on the oxidized Cu(110) surface retains S=1 at 0.4 K [19]. In addition, the magnetic anisotropy of FePc on the oxidized Cu(110) surface is reported to change to easy-axis from easy-plane [19] as we introduce in detail in chapter 3. The difference in the spin state of FePc adsorbed on the bare Cu(110) and the oxidized Cu(110) surface is attributed to the weaker molecule-substrate interaction for the latter [19]. FePc adsorbed on Au(111) is calculated by DFT calculations to retain S=1 [29]. Furthermore, the STS spectra of FePc taken at 0.4 K indicate that the spin is screened by the two stage Kondo effect [29]. It is proposed that the spin of FePc on Au(111) and the conduction electrons forms many-body doublet below 110-150 K, and many-body singlet below 2.6±1.4 K. We can interpret the result that the strength of interaction of FePc with the Au(111) substrate is between those of FePc with the bare Cu(110) and the oxidized Cu(110) substrates.

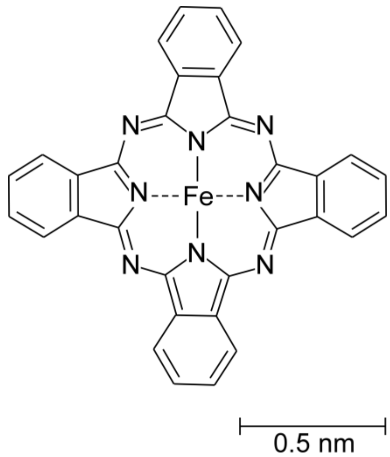

Figure 1.1 Molecular structure of FePc. The lengths and angles of the bonds were adopted from Ref. 31.

Figure 1.2 Schematic model of the arrangement of the molecule in the (a) β and (b) α polymorphs of FePc. Reprinted from Ref. 32, (The Figure is not included in the online version since it is not allowed by the copyright holder.)

1.3 Objective of the thesis

The objective of the thesis is to reveal influence of molecule-substrate and molecule-molecule interaction on the electronic and the spin state of the molecule. It is a general tendency that Cu is most reactive and Au is most inert from Au, Ag and Cu. Since the spin of FePc is retained on Au(111) [29] and quenched on

Cu(110) [19], it is intriguing whether the spin of the FePc on Ag substrate survives or not. The orientation of the substrate may also affect the spin state. To obtain further information on the effect of the molecule-substrate interaction, we investigated FePc adsorbed on Ag(111), Ag(110) and Ag(100) substrate. The influence of the molecule-molecule interaction on the spin state of the molecules was investigated by controlling the coverage of FePc on Ag(111), Ag(110), Ag(100) and Au(111) and measuring spatial distribution of the STS spectra. As we introduce in detail in chapter 4, FePc forms a lattice on Au(111) at a certain coverage, and the system is considered to be a two dimensional Kondo lattice [28]. Response of the electronic structure of FePc lattice formed on Au(111) to external magnetic fields of various amplitude and direction was examined to reveal the quantum state of the system.

In chapter 2, we introduce the apparatus and methods we used for the study. The spin and vibration excitations of FePc on Ag(111), Ag(110) and Ag(100) are described in chapter 3. We found that FePc molecules adsorbed directly on the Ag(111), Ag(110) and Ag(100) substrate do not show spin nor vibration related signals in the STS spectra. In contrast, the second layer FePc molecules on Ag(111), Ag(110) and Ag(100) substrate show both spin and vibration excitations in the STS spectra. The difference is discussed based on the electronic coupling between the molecules and the substrate. In chapter 4, we show that magnetic response of FePc lattice on Au(111) is anisotropic, and the spatial distribution of the electronic structure has longer periodicity than that of the molecular lattice under external magnetic field. We assign the ground of the system to an Ising type antiferromagnetic state based on the spectral evolution. Chapter 5 summarizes the thesis.

References

[1] C. Joachim, J. K. Gimzewski and A. Aviram, Nature **408**, 541 (2000).

[2] A. C. Hewson, *The Kondo Problem to Heavy Fermions*, 1st Pbk. Ed. with Corrections (Cambridge University Press, 1997).

[3] A. Danowitz, K. Kelley, J. Mao, J. P. Stevenson and M. Horowitz, Queue **10**, 10 (2012).

[4] E. Grochowski and R. D. Halem, IBM Syst. J. **42**, 338 (2003).

[5] C. A. F. Vaz, J. A. C. Bland, and G. Lauhoff, Rep. Prog. Phys. **71**, 056501 (2008).

[6] M. Baibich, J. Broto, A. Fert, F. Van Dau, F. Petroff, P. Etienne, G. Creuzet, A. Friederich, and J. Chazelas, Phys. Rev. Lett. **61**, 2472 (1988).

[7] G. Binasch, P. Grünberg, F. Saurenbach, and W. Zinn, Phys. Rev. B **39**, 4828 (1989).

[8] G. Binnig, H. Rohrer, C. Gerber, and E. Weibel, Physica B+C **109–110, Part 3**, 2075 (1982).

[9] G. Binnig, H. Rohrer, C. Gerber, and E. Weibel, Appl. Phys. Lett. **40**, 178 (1982).

[10] G. Binnig, H. Rohrer, C. Gerber, and E. Weibel, Phys. Rev. Lett. **50**, 120 (1983).

[11] G. Binnig, K. H. Frank, H. Fuchs, N. Garcia, B. Reihl, H. Rohrer, F. Salvan, and A. R. Williams, Phys. Rev. Lett. **55**, 991 (1985).

[12] A. J. Heinrich, J. A. Gupta, C. P. Lutz, and D. M. Eigler, Science **306**, 466 (2004).

[13] B. C. Stipe, M. A. Rezaei, and W. Ho, Science **280**, 1732 (1998).

[14] J. Lambe and R. C. Jaklevic, Phys. Rev. **165**, 821 (1968).

[15] C. F. Hirjibehedin, C. P. Lutz, and A. J. Heinrich, Science **312**, 1021 (2006).

[16] C. F. Hirjibehedin, C.-Y. Lin, A. F. Otte, M. Ternes, C. P. Lutz, B. A. Jones, and A. J. Heinrich, Science **317**, 1199 (2007).

[17] X. Chen, Y.-S. Fu, S.-H. Ji, T. Zhang, P. Cheng, X.-C. Ma, X.-L. Zou, W.-H. Duan, J.-F. Jia, and Q.-K. Xue, Phys. Rev. Lett. **101**, 197208 (2008).

[18] A. F. Otte, M. Ternes, K. von Bergmann, S. Loth, H. Brune, C. P. Lutz, C. F. Hirjibehedin, and A. J. Heinrich, Nat. Phys. **4**, 847 (2008).

[19] N. Tsukahara, K. Noto, M. Ohara, S. Shiraki, N. Takagi, Y. Takata, J. Miyawaki, M. Taguchi, A. Chainani, S. Shin, and M. Kawai, Phys. Rev. Lett. **102**, 167203 (2009).

[20] S. Loth, C. P. Lutz, and A. J. Heinrich, New J. Phys. **12**, 125021 (2010).

[21] S. Loth, K. von Bergmann, M. Ternes, A. F. Otte, C. P. Lutz, and A. J. Heinrich, Nat. Phys. **6**, 340 (2010).

[22] T. Schuh, T. Miyamachi, S. Gerstl, M. Geilhufe, M. Hoffmann, S. Ostanin, W. Hergert, A. Ernst, and W. Wulfhekel, Nano Lett. **12**, 4805 (2012).

[23] T. Miyamachi, T. Schuh, T. Märkl, C. Bresch, T. Balashov, A. Stöhr, C. Karlewski, S. André, M. Marthaler, M. Hoffmann, M. Geilhufe, S. Ostanin, W. Hergert, I. Mertig, G. Schön, A. Ernst, and W. Wulfhekel, Nature **503**, 242 (2013).

[24] T. Choi, M. Badal, S. Loth, J.-W. Yoo, C. P. Lutz, A. J. Heinrich, A. J. Epstein, D. G. Stroud, and J. A. Gupta, Nano Lett. **14**, 1196 (2014).

[25] I. G. Rau, S. Baumann, S. Rusponi, F. Donati, S. Stepanow, L. Gragnaniello, J. Dreiser, C. Piamonteze, F. Nolting, S. Gangopadhyay, O. R. Albertini, R. M. Macfarlane, C. P. Lutz, B. A. Jones, P. Gambardella, A. J. Heinrich, and H. Brune, Science **344**, 988 (2014).

[26] J. Li, W.-D. Schneider, R. Berndt, and B. Delley, Phys. Rev. Lett. **80**, 2893 (1998).

[27] V. Madhavan, W. Chen, T. Jamneala, M. F. Crommie, and N. S. Wingreen, Science **280**, 567 (1998).

[28] N. Tsukahara, S. Shiraki, S. Itou, N. Ohta, N. Takagi, and M. Kawai, Phys. Rev. Lett. **106**, 187201 (2011).

[29] E. Minamitani, N. Tsukahara, D. Matsunaka, Y. Kim, N. Takagi and M. Kawai, Phys. Rev. Lett. **109**, 086602 (2012).

[30] A. Mugarza, R. Robles, C. Krull, R. Korytár, N. Lorente and P. Gambardella, Phys. Rev. B **85**, 155437 (2012).

[31] J. F. Kirner, W. Dow, and W. R. Scheidt, Inorg. Chem. **15**, 1685 (1976).

[32] C. Ercolani, C. Neri, and P. Porta, Inorg. Chim. Acta **1**, 415 (1967).

[33] R. P. Linstead and J. M. Robertson, J. Chem. Soc. 1736 (1936).

[34] B. W. Dale, R. J. P. Williams, C. E. Johnson, and T. L. Thorp, J. Chem. Phys. **49**, 3441 (1968).

[35] M. Evangelisti, J. Bartolomé, L. de Jongh, and G. Filoti, Phys. Rev. B **66**, (2002).

[36] C. G. Barraclough, R. L. Martin, S. Mitra, and R. C. Sherwood, J. Chem. Phys. **53**, 1643 (1970).

Chapter 2

Apparatus and Methods

In the thesis, scanning tunneling microscopy (STM) and spectroscopy (STS) were utilized to investigate the real-space geometric structure and local electronic of the sample, respectively. High resolution electron energy loss spectroscopy (HREELS) is also utilized in our study to reveal molecule-substrate interaction. In this chapter, we describe the mechanism and apparatus for these techniques. The sample preparation method is also described.

2.1 STM

STM is a type of scanning probe microscope in which a sharp probe tip scans the sample surface to obtain the image of the surface structure. STM utilizes tunneling effect of an electron to control the tip-sample separation. Using STM, we can also conduct local spectroscopy called scanning tunneling spectroscopy (STS). In this section, we introduce the mechanism of STM, and describe the apparatus for STM we used in the study.

2.1.1 Mechanism of scanning tunneling microscopy and spectroscopy

Components of a scanning tunneling microscope

The sample measured by STM must be conductive (i.e. metal or semiconductor). A metal probe tip and the conductive sample are set close to each other, in a distance of ~ 1 nm. Both the tip and the sample are connected to electrodes (which are separated each other) so that bias voltage, V, can be applied between them. The tunneling current, I, which flows between the tip and the sample is measured and utilized to operate STM. Schematic image of electronics of STM is shown in Fig. 2.1. The relative position between the tip and the sample is controlled by using piezoelectric drive elements. (In our system, the sample is fixed to an immobile stage, and the tip is fixed on a piezoelectric driven stage.) The position of the tip stage is controlled three dimensionally by applying voltage on x, y and z piezoelectric drive elements. As described below, the tunneling current depends on the distance between the tip and the sample, and the absolute value increases (decreases) when the separation between the tip and the sample decreases (increases). Therefore, supposing that the surface of the sample is flat and parallel to the xy plane, the tunneling current only depends on the z positon of the tip (and the applied voltage of the z piezoelectricity). There is a feedback loop circuit which change the voltage of z piezoelectricity to make the tunneling current I a given value. By switching the feedback loop on, the distance between the tip and the sample can be maintained constant. If the surface of the sample is not flat, the value of z which make the tunneling current a given value becomes the function of x and y. By scanning the tip in x and y direction with the feedback loop on, and recording x,y and z values, information on the three dimensional structure of the sample can be obtained. The tunneling current also depends on the local density of states of the sample. By fixing the tip positon, and measuring the dependence of the tunneling current (I) or its derivative (dI/dV) on V, spectrum which reflect the local density of states can be obtained. The dI/dV is measured using lock-in amplification technique. The lock-in modulation voltage can be imposed on the sample bias, and the tunneling current is also read by the lock-in amplifier. The applied bias voltage between the sample and the tip, the tunneling current, the voltage applied to x, y and z piezoelectricity and the amplified dI/dV signal are all received and recorded by a computer during the operation of STM.

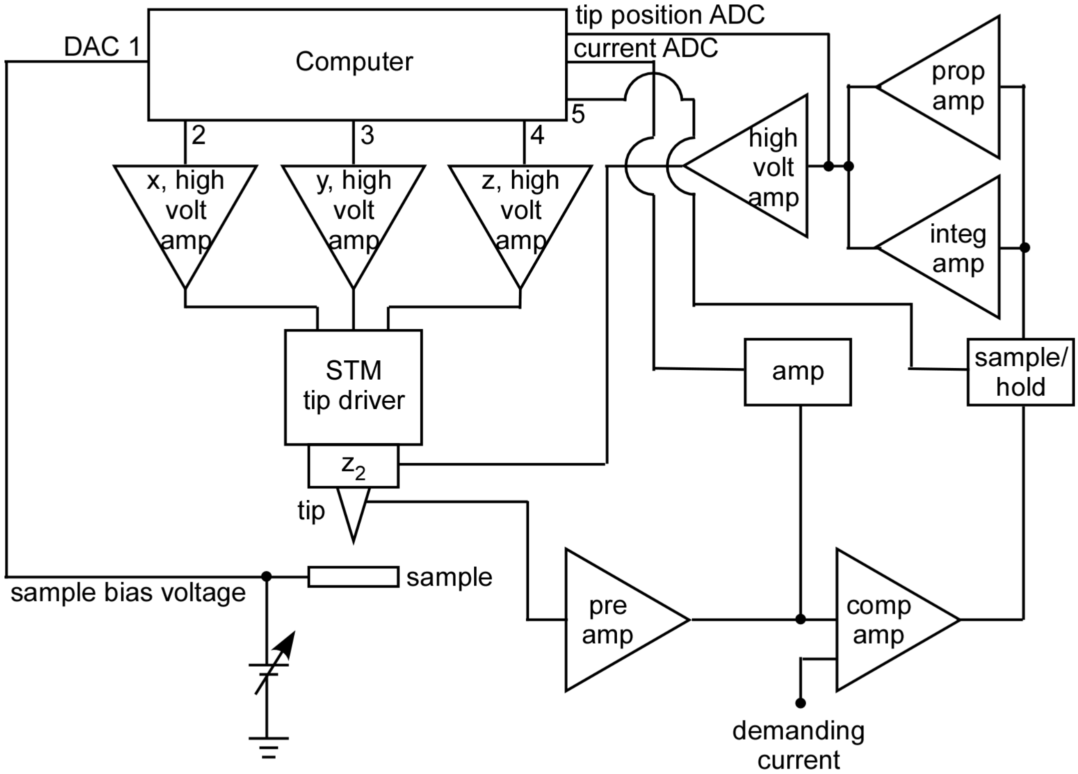

Figure 2.1 Electronics for STM. We referred FIG. 15 in Ref. 1 to draw the image. The image is modified from the original one to fit the system we employed. DAC: digital to analog converter, ADC: analog to digital converter

Model of tunneling current for planer metal-vacuum-metal junction

Sensitivity of tunneling current on the separation of a tunneling junction is shown using a simple model. Tunneling of planer metal-vacuum-metal junction is described by using one dimensional model. Wave function of an electron with energy E in a potential given in Fig. 2.2 is obtained by solving a time-independent Schrödinger equation,

$$\left(-\frac{\hbar^2}{2m_e}\frac{d^2}{dx^2}+V\right)\Psi = E\Psi$$

where

$$\begin{aligned} V &= 0 \ (x < 0, s < x) \\ &= V_0 (0 < x < s), \end{aligned}$$

$\hbar$ is the Planck constant devided by 2π and m_e is the mass of an electron. The wave function in region1 $(x < 0)$, region2 $(0 < x < s)$ and region3 $(x < s)$ is expressed as,

$$\Psi_1 = \mathrm{A}e^{ikx} + \mathrm{B}e^{-ikx},$$
$$\Psi_2 = \mathrm{C}e^{\kappa x} + \mathrm{D}e^{-\kappa x},$$
$$\Psi_3 = \mathrm{E}e^{ikx} + \mathrm{F}e^{-ikx},$$

respectively where

$$k = \sqrt{2m_e(V_0 - E)}/\hbar\,,$$
$$\kappa = \sqrt{2m_e(E - V_0)}/\hbar.$$

When there is no impinging electron from right side (i.e. F = 0), wave matching conditions ($\Psi_1(x=0) = \Psi_2(x=0)$, $\left.\frac{d\Psi_1}{dx}\right|_{x=0} = \left.\frac{d\Psi_2}{dx}\right|_{x=0}$, $\Psi_2(x=s) = \Psi_3(x=s)$ and $\left.\frac{d\Psi_2}{dx}\right|_{x=s} = \left.\frac{d\Psi_3}{dx}\right|_{x=s}$) gives

$$\left|\frac{\mathrm{E}}{\mathrm{A}}\right|^2 = \frac{1}{1 + \frac{(k^2+\kappa^2)^2}{4k^2\kappa^2}\sinh^2(\kappa s)}$$
$$\sim \frac{16k^2\kappa^2}{(k^2+\kappa^2)^2} e^{-2\kappa s} \propto e^{-2\kappa s}.$$

When the barrier height $V_0 - E$ is 4 eV and s = 1 nm, changes of the tunneling probability |E/A|^2 near one order of magnitude is estimated for Δs = 0.1 nm.

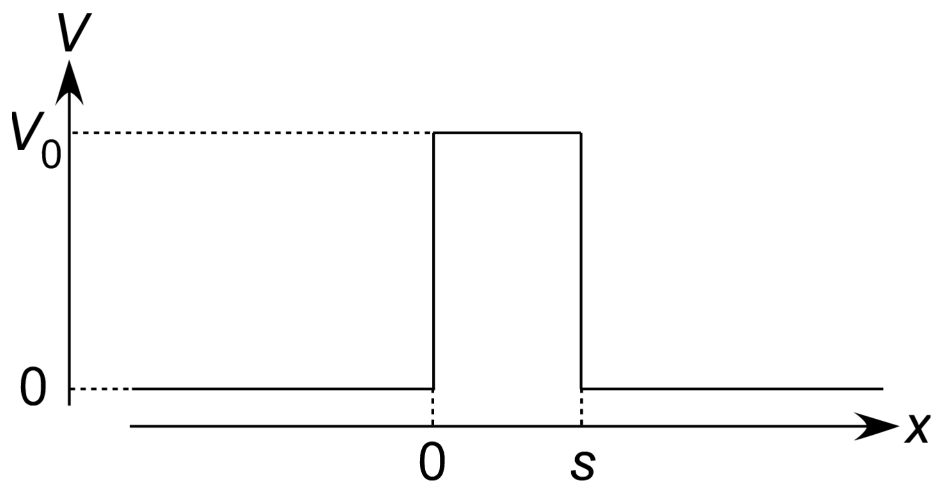

Figure 2.2 Schematic diagram of the one dimensional potential.

Model of tunneling current for STM configuration

Tunneling current in the configuration of STM (see Fig. 2.3) is often evaluated using method by Tersoff and Hamann [2]. They use Bardeen's formalism of tunneling current [3],

$$I = \frac{2\pi e}{\hbar}\sum_{\mu,\nu} f(E_\mu)[1 - f(E_\nu - eV)]\left|M_{\mu\nu}\right|^2 \delta(E_\mu - E_\nu),$$

where $M_{\mu\nu}$ is the tunneling matrix between a state of the tip, μ, and that of the sample, ν, f is the Fermi-Dirac function, V is the applied bias voltage of the sample with respect to the tip, $E_{\mu(\nu)}$ is the energy of the state $\mu(\nu)$ when the tunneling is absent. $M_{\mu\nu}$ is calculated from wave function of state μ and ν in the tunnel region, ψ_μ and ψ_ν, as

$$M_{\mu\nu} = \frac{\hbar}{2m_e}\int d\boldsymbol{S}\cdot\left(\psi_\mu{}^*\nabla\psi_\nu - \psi_\nu{}^*\nabla\psi_\mu\right),$$

where the integral is taken over the entire surface between the tip and the sample. In their method, Tersoff and Hamann consider the case for small V, and rewrite the formula for the tunneling current as,

$$I = \frac{2\pi}{\hbar}e^2 V\sum_{\mu,\nu}\left|M_{\mu\nu}\right|^2 \delta(E_\mu - E_F)\delta(E_\nu - E_F),$$

where E_F is the Fermi energy. They represent the tip apex by a spherical potential with radius of curvature R and the center at position $\boldsymbol{r_0}$, and take

$$\psi_\mu = \Omega_t{}^{-1/2} c_t \kappa R e^{\kappa R}(\kappa)|\boldsymbol{r} - \boldsymbol{r_0}|^{-1} e^{-\kappa|\boldsymbol{r}-\boldsymbol{r_0}|}$$

as the wave function of the tip where Ω_t is the volume of the tip, $\kappa = (2m_e\phi)^{1/2}/\hbar$, ϕ is the work function (which is assumed to be same for the tip and the sample for simplicity). Then, for the periodic surface, $M_{\mu\nu}$ and I are evaluated analytically as,

$$M_{\mu\nu} = \frac{\hbar}{2m_e} 4\pi\kappa^{-1}\Omega_t{}^{-1/2}\kappa R e^{\kappa R}\psi_\nu(\boldsymbol{r_0})$$

and

$$I = \frac{32\pi^3}{\hbar}e^2 V\phi^2 n_t(E_\mathrm{F})R^2\kappa^{-4}e^{2\kappa R}\sum_\nu|\psi_\nu(\boldsymbol{r_0})|^2\delta(E_\nu - E_F).$$

n_t is the density of states per unit volume of the tip and $|\psi_\nu(\boldsymbol{r_0})|^2$ is the density of states of the sample evaluated at the center of the curvature of the approximated tip.

Since $|\psi_\nu(\boldsymbol{r_0})|^2 \propto e^{-2\kappa(R+s)}$ where s is the vacuum gap, the tunneling current is also proportional to $e^{-2\kappa s}$ in the configuration of STM.

By extending their results, tunneling current for large V is often expressed by the shift of the density of states [4] as,

$$I \propto \int_0^{eV} n_s(E) n_t(-eV + E) T(E, eV) dE \qquad (2.1)$$

where

$$T(E, eV) = \exp\left\{-2(s+R)\left[\frac{2m_e}{\hbar^2}\left(\frac{\phi_t + \phi_s}{2} + \frac{eV}{2} - E\right)\right]^{1/2}\right\}$$

is the transmission factor calculated with WKB method, n_s is the local density of states of the sample, $\phi_{t(s)}$ is the work function of the tip(sample). Schematic image of the energy alignment is shown in Fig. 2.4.

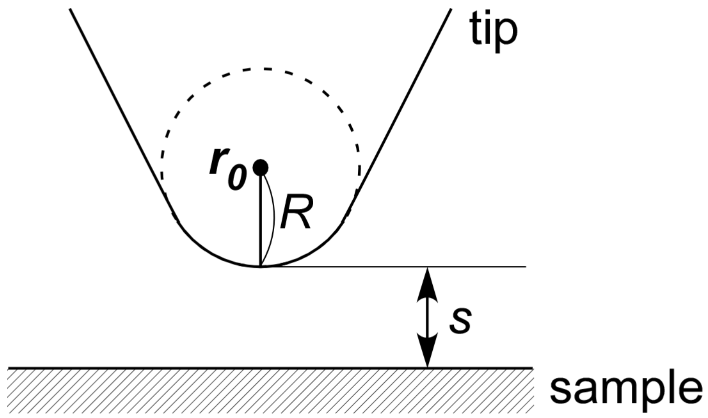

Figure 2.3 Geometrical arrangement of the tip and the sample in STM.

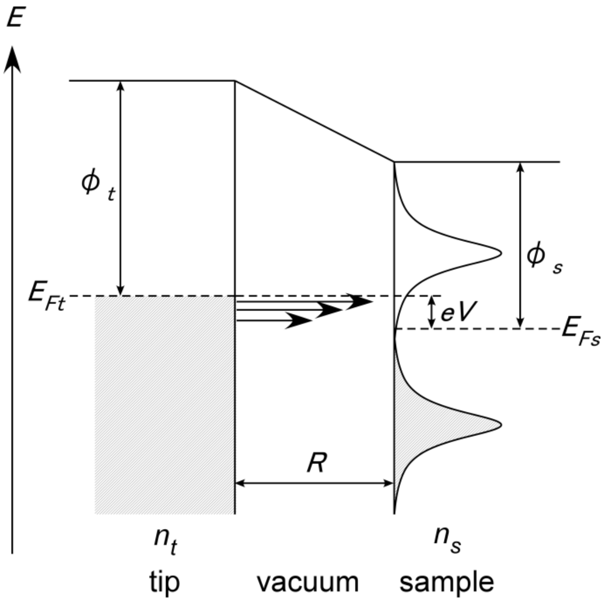

Fig. 2.4 Energy alignment of the tip and the sample in STM. $E_{Fs(t)}$ represents the Fermi energy of the sample (tip).

Mechanism of scanning tunneling spectroscopy

Differentiating above expression for the tunneling current (eq. (2.1)) by V, and supposing $dn_t/dV = 0$, Hamers obtained [5]

$$\frac{dI}{dV} \propto n_s(eV)n_t(0)T(eV,eV) + \int_0^{eV} n_s(E)n_t(-eV+E)\frac{dT(E,eV)}{dV}dE.$$

$T(E,eV)$ increases monotonically with V, and the last term is considered to give smooth background. The structure in dI/dV spectra is usually attributed to the first term: the local density of states of the sample.

Lock-in amplification technique is often used to measure dI/dV. In the technique, sinusoidal modulation voltage V_{mod} with frequency ω is imposed on the sample bias. Then, the tunneling current is expressed using Taylor expansion as

$$I\left(V_s + V_{mod}sin(\omega t)\right)$$
$$\cong I(V_s) + \left.\frac{dI}{dV}\right|_{V=V_s} V_{mod}sin(\omega t) + \frac{1}{2}\left.\frac{d^2I}{dV^2}\right|_{V=V_s} {V_{mod}}^2\left(\frac{1}{2} - \frac{1}{2}sin\left(2\omega t + \frac{\pi}{2}\right)\right) + \cdots \ .$$

The tunneling current is transferred as a signal voltage $V_{sig} \propto I$ to the lock-in amplifier. In the detection process, the signal is multiplied by a reference sinusoidal voltage $V_{ref}sin(\omega t)$ which has the same frequency with the modulation voltage. Then, the dc component of the yield, $V_{sig}V_{ref}sin(\omega t)$, is proportional to

$dI/dV|_{V=V_S}$. The yield is processed through low-pass filter so that we obtain the dc component $\propto dI/dV|_{V=V_S}$.

Mechanism of inelastic electron tunneling spectroscopy

In the description above, the energy of electron before and after tunneling is assumed to be conserved, i.e., the tunneling is elastic. Inelastic electron tunneling in which a tunneling electron causes an excitation of energy $\hbar\omega$ and loses the same energy during tunneling is also possible. At very low temperature, inelastic process only occurs when the absolute value of the applied bias voltage $|V|$ is larger than the excitation energy divided by the elemental charge, e, since it is impossible for an electron to tunnel into an occupied state. The schematic energy diagram of inelastic tunneling is shown in Fig. 2.5a.

The addition of inelastic process at $|V| = \hbar\omega/e$ causes change in the tunneling probability at the voltage. Therefore, step like structure appear in the dI/dV spectra as schematically shown in Fig. 2.5b. From the point of view of interpretation of the dI/dV spectra, the energy of the excitation can be extracted from the position of the step. This method is called inelastic electron tunneling spectroscopy (IETS). Spin [6] and vibration [7] excitations of individual atoms or molecules have been measured using the method.

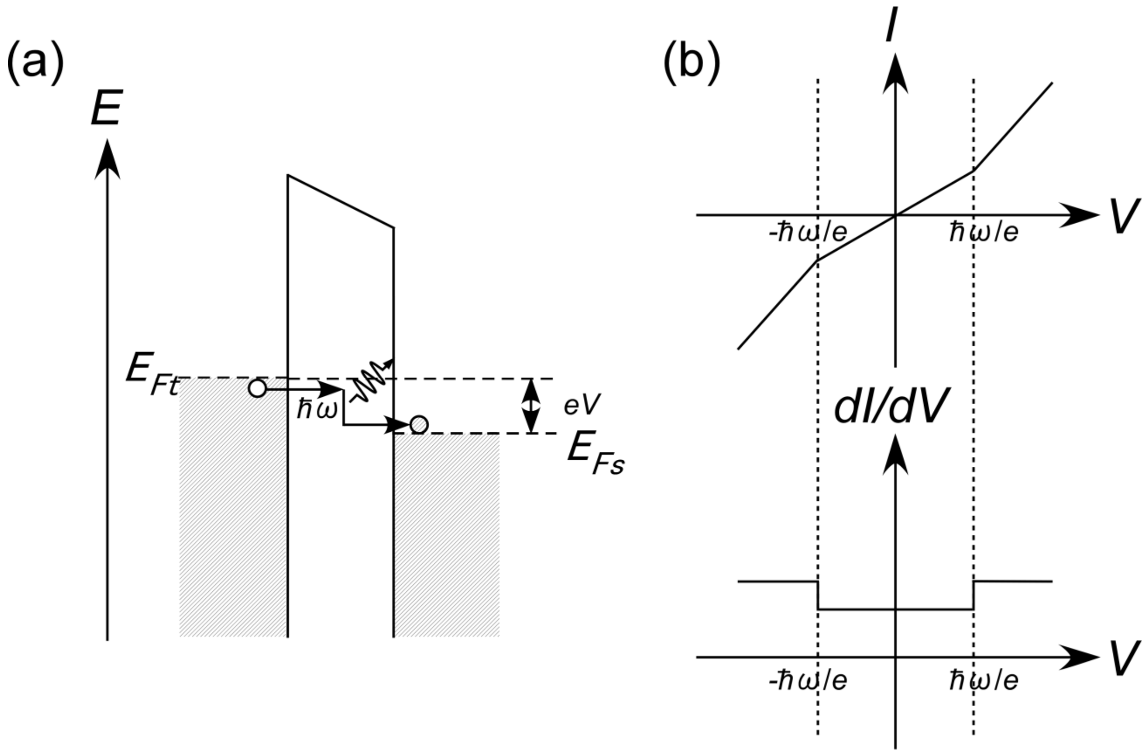

Figure 2.5 Schematic image of (a) inelastic electron tunneling process and (b) *I*-*V* and d*I*/d*V*-*V* spectra when the tunneling electrons interact with an oscillator with energy $\hbar\omega$.

2.1.2 Apparatus for STM measurement

We used two ultrahigh vacuum systems each of which is equipped with a low-temperature scanning tunneling microscope (STM). One is USM1300 ^{3}He model and the other is USM1300 VTI model of Unisoku company. Those two have different cooling system as described below. The cryostats are equipped with superconducting magnets, using which we can apply magnetic field parallel or perpendicular to the sample surface.

Ultrahigh vacuum system

Schematic image of the ultrahigh vacuum system is shown in Fig. 2.6. The ultrahigh vacuum system consists of a load lock chamber, a preparation chamber, a stock chamber and a measurement chamber. Those chambers are connected through gate valves, and the samples and the tips can be transferred between them using transfer rods. A turbo molecular pump is used to evacuate load lock chamber after introduction of samples and tips from outside of the UHV system. The pressures of the preparation, the stock and the measurement chamber is maintained below 1×10^{-10} Torr by the combination of a turbo molecular pump, two ion sputtering pumps, and two titan sublimation pumps.

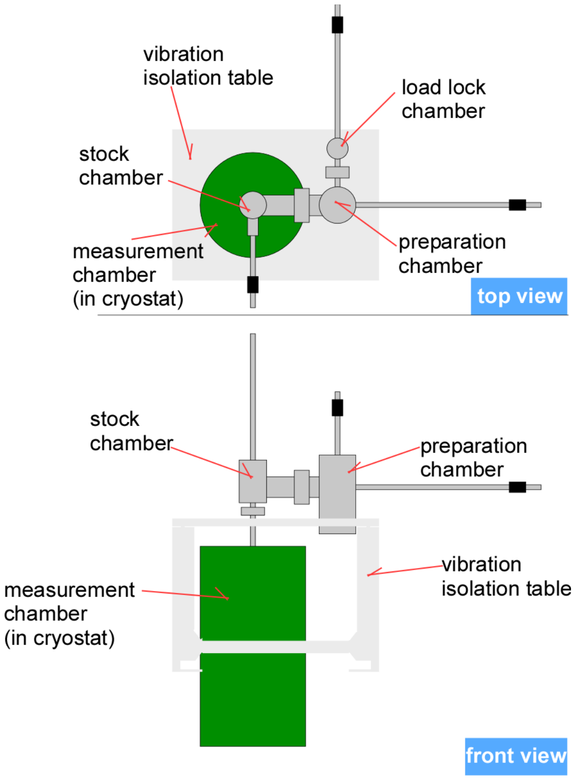

Figure 2.6 Schematic image of the UHV system for STM measurements.

Cooling system

The cooling system is different for the ^{3}He model and the VTI model. Schematic image of the measurement chamber and the surrounding cooling system is shown in Fig. 2.7 for each model.

In the cooling system of the ^{3}He model, the STM chamber and the ^{3}He chamber is thermally isolated from the outside ^{4}He tank by a vacuum layer. The ^{3}He gas acts as the thermal exchange medium to cool the STM unit. To operate STM at the lowest temperature (400 mK), the ^{3}He gas is liquefied by thermal contact with ^{4}He gas in 1 K pot at first. The ^{4}He gas flow into the 1 K pot through the needle valve, and is cooled down to ~1.4 K by pumping using a rotary pump. At the temperature, the ^{3}He gas is liquefied until its vapor pressure becomes ~30 Torr. In our system, ~18 L ^{3}He gas is liquefied at this stage. After the liquefaction, the ^{3}He gas is pumped by the sorption pump by cooling the pump using the ^{4}He flow. It results in further decrease of the temperature of the liquefied ^{3}He. Thus, the lowest temperature of the STM unit is achieved. The period that the temperature can be kept is ≳ 24 hours. Without pumping of the ^{3}He gas, the temperature of the sample becomes 2-3 K.

The VTI model is equipped with the variable temperature insert (VTI). The flow of ^{4}He into the VTI is controlled by the needle valve. The heater to heat the flow is installed near the needle valve. The temperature of the sample can be controlled between 2.5 K and 50 K by controlling the flow and heating power. In this study, the ^{4}He gas inside the VTI was only utilized as the thermal exchange gas between the STM chamber and the ^{4}He tank without pumping. The sample temperature of 6 K was achieved in this condition.

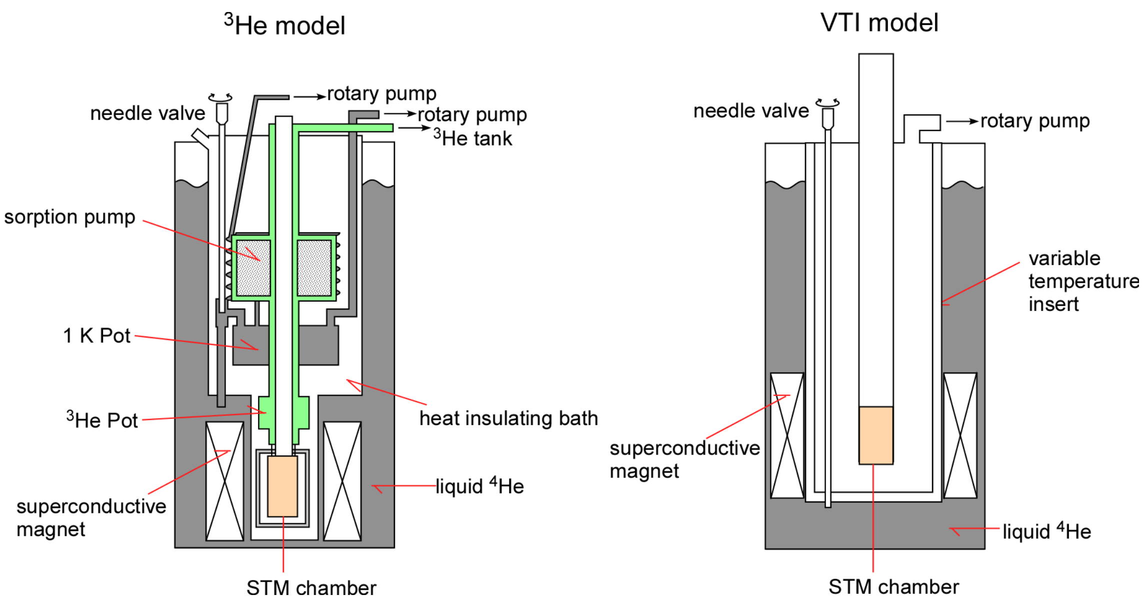

Figure 2.7 Cooling systems for Unisoku USM1300 (left) ^{3}He model and (right) VTI model. The images were re-drawn based on those in Ref. [8]

Application of magnetic field

Magnetic fields were applied parallel or perpendicular to the substrate using super conducting magnet equipped inside the cryostat. In this thesis, all STM measurements under magnetic field were conducted using the ^{3}He model. The direction of the magnetic field is fixed to the cryostat. The direction of the magnetic field (perpendicular or parallel to the substrate) was switched by changing the cryostat, i.e. two cryostats were used. The angle of the in-plane magnetic field relative to the STM scanning direction was determined using the method described in Appendix A. The superconducting magnets are capable of applying up to 11 T (7 T) perpendicular (parallel) to the substrate.

Preparation of the STM tip

Tungsten tip made using electro-chemical etching method with drop-off technique [9] is often adopted as the STM tip. Schematic image of the drop off technique is shown in Fig. 2.8. When the weight of the portion of the tungsten below air-water interface exceeds the tensile which holds it, the lower part drop off and the sharp tips are made. We made the probe tip from tungsten wire with 0.3 mm φ using ready-made device for electro-chemical etching produced by JEOL Ltd. (TM-59060). The setup of the device is similar to that described in Ref. [10]. An electric circuit to detect the drop-off and to stop the etching is incorporated in the device. Before etching, the tungsten wire was cut and mechanically polished using plastic files with grain diameter 12 and 3 μm. The wire was then cleaned in ethanol by using ultrasonic cleaning process. After that, the wire was etched in 2M NaOH, and rinsed in a hot water and ethanol. Then, the tip was introduced in the ultrahigh vacuum chamber. To remove the oxide layer, the tip was annealed or observed by field ion microscope (FIM) in the chamber. Further conditioning was done in the STM setup by observing Au(111) surface with the prepared tip. Application of high bias voltage ~few eV and intentional impinging of the tip on the surface were made to change the composition and shape of the tip apex. The tip was validated by observing surface states of Au(111) surface.

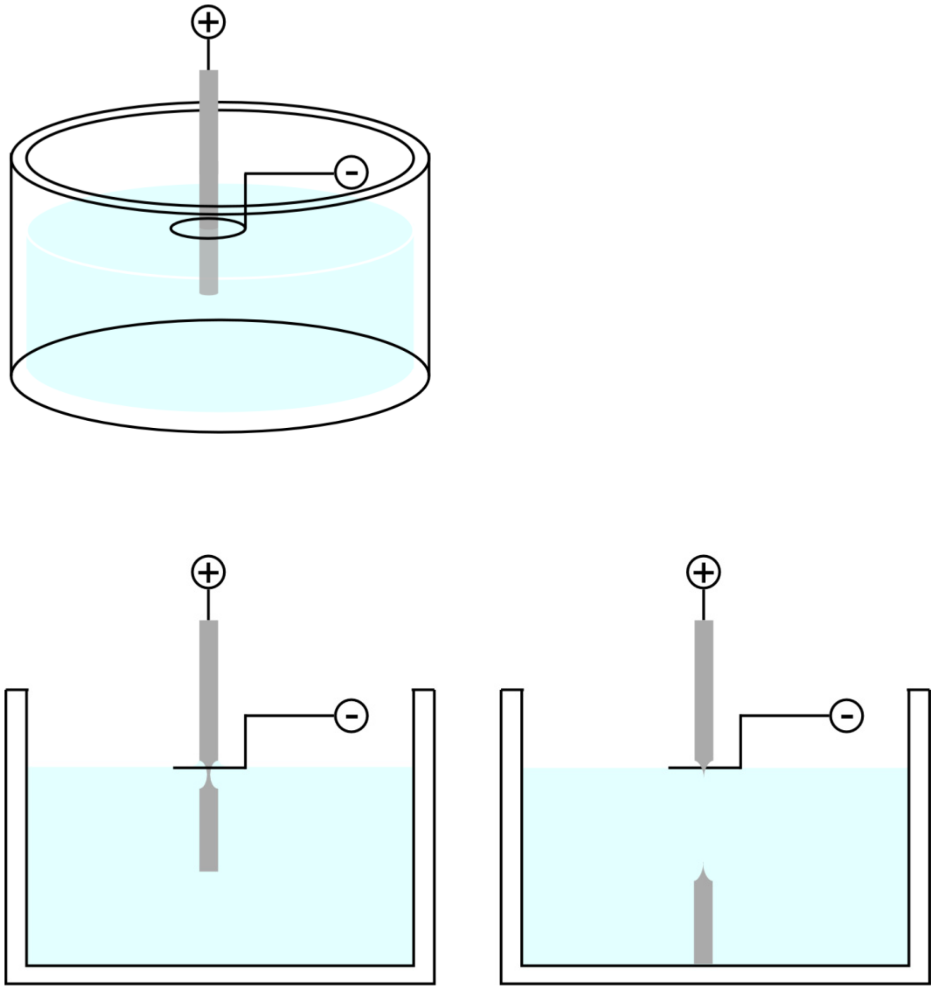

Figure 2.8 Schematic image of the drop off technique to prepare STM tips.

2.2 HREELS

Using HREELS, we can measure vibrational spectra of molecules adsorbed on metal surfaces. The selection rules of HREELS are utilized to identify the molecular orientation. In the thesis, we used HREELS spectra to investigate the adsorption state of the molecules. In this section, we introduce the mechanism of HREELS, and the apparatus for HREELS used in the study.

2.2.1 Mechanism of HREELS

HREELS measure loss of electron energy reflected or scattered by the sample surface [11]. Schematic image of HREELS system is depicted in Fig. 2.9. The electron emitted from a filament is passed through two electrostatic lenses, and made monochromatic. The sample is set in front of the exit of the monochromater so that the electron interact with the sample. Electrostatic lenses similar to those in the monochromater are used as an analyzer to pass the electron with a certain energy which is scattered to the direction of the analyzer. The number of the electron is counted by using a channel electron multiplier at the end of the analyzer. The arrangement of the monocromator, the sample, and the analyzer is variable, so that we can measure the dependence of the energy loss probability on the scattering angle, which helps the identification of the origin of the energy losses as described below.

The mechanism of inelastic electron scattering is classified into three types: dipole scattering, resonant scattering and impact scattering. Each of which is characterized by dependence of the scattering cross section on the energy of impinging electrons and the angular distribution of the scattered electrons. Especially, selection rule for dipole scattering mechanism only allows excitation of totally symmetric vibration modes [11].

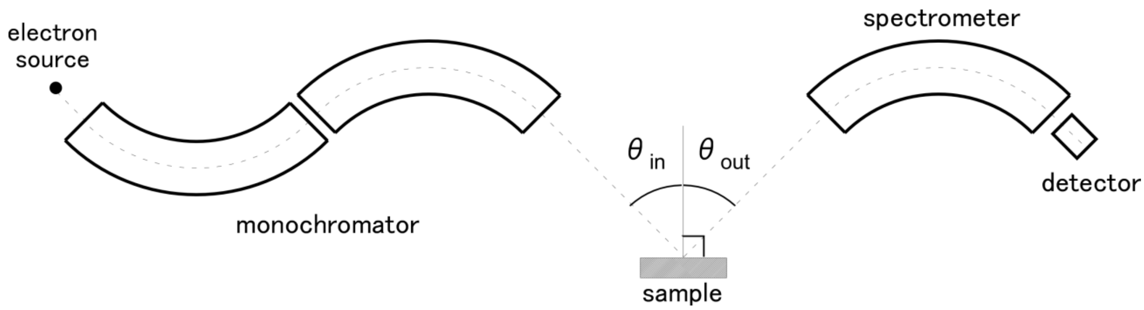

Figure 2.9 Schematic configuration of HREELS system

2.2.2 Apparatus for HREELS measurement

Ultrahigh vacuum system for HREELS measurement consists of a preparation chamber and an analysis chamber. The sample can be transferred between the two chambers. The analysis chamber is equipped with an Auger-LEED system, and HREELS system, the former at the upper part of the chamber, and the latter at the bottom of the chamber as schematically shown in Fig. 2.10. Each chamber is equipped with a turbo molecular pump, an ion pump and a titan sublimation pump, and the background pressure is kept $\lesssim 2\times10^{-10}$ Torr.

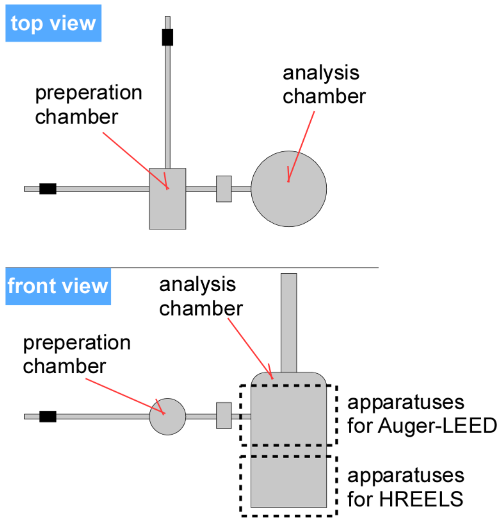

Figure 2.10 Shematic image of the UHV system for HREELS measurements

2.3 Sample preparation method

We used Ag(111), Ag(110), Ag(100) and Au(111) single crystal surfaces as substrates. The method for sample preparation was same for all substrates. First, the substrate was cleaned by repeating Ar ion (0.6 keV) sputtering and annealing several times. Typical pressure of Ar gas while sputtering was 2×10^{-6} Torr, and the sample current was ~2 μA. The sample was annealed to 700 K by electron bombardment heating (radiative heating) in the apparatus for STM (HREELS) respectively. FePc molecules were deposited onto the sample kept at room temperature by heating a ceramic cell which contains powder of the molecule at 590 K. Schematic image of the depositor is shown in Fig. 2.11. The coverage of the molecule is measured from STM image in STM measurements. We sometimes conducted additional deposition of FePc after confirmation of the coverage. In HREELS measurement, the coverage was measured using Auger spectroscopy by comparing intensity of signals from Ag and C. The coverage was measured after HREELS measurement to avoid contamination.

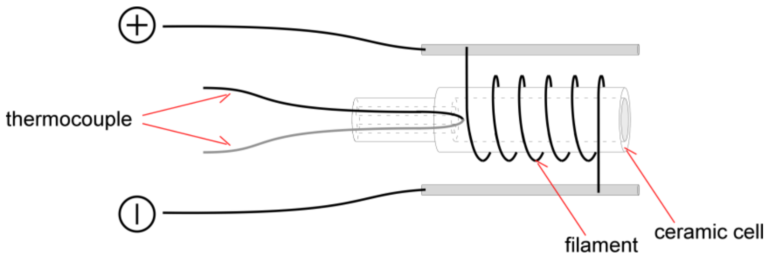

Figure 2.11 Schematic structure of the depositor

References

[1] Y. Kuk and P. J. Silverman, Rev. Sci. Instrum. **60**, 165 (1989).

[2] J. Tersoff and D. R. Hamann, Phys. Rev. B **31**, 805 (1985).

[3] J. Bardeen, Phys. Rev. Lett. **6**, 57 (1961).

[4] R. Wiesendanger, *Scanning Probe Microscopy and Spectroscopy: Methods and Applications* (Cambridge University Press, 1994).

[5] R. J. Hamers, Annu. Rev. Phys. Chem. **40**, 531 (1989).

[6] A. J. Heinrich, J. A. Gupta, C. P. Lutz, and D. M. Eigler, Science **306**, 466 (2004).

[7] B. C. Stipe, M. A. Rezaei, and W. Ho, Science **280**, 1732 (1998).

[8] Unisoku, manual

[9] P. J. Bryant, H. S. Kim, Y. C. Zheng, and R. Yang, Rev. Sci. Instrum. **58**, 1115 (1987).

[10] J. P. Ibe, P. P. B. Jr, S. L. Brandow, R. A. Brizzolara, N. A. Burnham, D. P. DiLella, K. P. Lee, C. R. K. Marrian, and R. J. Colton, J. Vac. Sci. Technol., A **8**, 3570 (1990).

[11] H. Ibach and D. L. Mills, *Electron Energy Loss Spectroscopy and Surface Vibrations* (Academic Press, New York, 1982).

Chapter 3

Spin and vibration excitations of FePc/Ag(111), Ag(110), Ag(100)

Chapter 3 is not included in the online version because it includes unpublished data.

Chapter 4

Collective magnetic state of FePc/Au(111)

Chapter 4 is not included in the online version because it includes unpublished data.

Chapter 5

Summary and Outlook

In this study, we examined the low energy structure, adsorption structure and their relation of iron phthalocyanine molecules on Ag(111), Ag(110), Ag(100) and Au(111) surface.

The iron phthalocyanine which adsorbed directly on the Ag(111), Ag(110) and Ag(100) surface doesn't show any noticeable structure i.e. spin excitation, vibration excitation nor Kondo resonance in the narrow range dI/dV spectra. It is plausible that the spins of them are quenched due to strong hybridization with the Ag substrate. The existence of such interaction between the Fe of FePc and Ag substrate is confirmed by vibrational energy shift using high resolution electron energy loss spectroscopy for FePc/Ag(111). The molecules in the second layer on Ag(111), Ag(110) and Ag(100) show several conductance steps. They were assigned to spin and vibration excitations. In the case of FePc/Ag(111), the energy position depends on the rotation angle of the second layer molecule from the first layer molecule below. On Ag(110) and Ag(100), the excitation energies also depend on the local configurations.

Iron phthalocyanine molecules inside molecular lattice on Au(111) show double dip structure without magnetic field. The spectral dependence on the magnetic field is not spatially uniform, and adjacent molecules show different responses; the molecules show double dip structure and single dip structure alternately under magnetic field of 3 T along one in-plane molecular axis. The spectral response to magnetic field is also anisotropic. The spectra less response to the magnetic field applied parallel to the other two molecular axes. We assigned the ground state of the FePc molecular lattice to an Ising type antiferromagnetic state. The spectral dependence on the magnetic field was analyzed using a phenomenological method. From the analysis, coexistence of the Kondo effect and exchange interaction between the molecular spins is indicated.

Further studies using macroscopic measurement method and theoretical calculation may compensate the current study. Quenches of spin of the first layer FePc on silver surfaces may be confirmed by PES measurement. Macroscopic properties of FePc lattice on Au(111) is also intriguing. Information on dependence of the magnetization and the electric resistance of the system on external magnetic field will help theoretical investigation on the system. First principles calculations will also help us to interpret the obtained results. Some question is remaining including

-what kind of interaction between the substrate and the molecule quenches the spin of the FePc in the first layer on silver surfaces?, and

-what kind of difference in the electronic structure lead to different spin and vibration excitation energies of the FePc in the second layer on silver surfaces? Those questions will be answered by calculating the electronic structure of the system. The magnetic evolution of the bound state of the FePc lattice on Au(111) should also be explained theoretically using more precise model including the influence of the Kondo effect explicitly.

The current study deepens our understanding on the electronic and the spin state, their sensitivity on the geometrical structure of molecules at the interface. The study will also encourage theoretical and experimental investigation on two dimensional Kondo lattice.

Appendix A: Determination of the direction of the magnetic field to the scanning direction

The direction of the in-plane magnetic field was determined against x and y scan direction of STM piezoelectric drive so that we can signify the direction of magnetic field in STM image. Single crystal of gold with notation of crystal direction was used as a sample to know the direction. The sample was fixed on a sample holder which can rotate by 120° on sample stage as shown in Fig. A.1. Four procedures were taken.

1. The direction of the in-plane magnetic field against the ultrahigh vacuum system was measured.
2. The direction of the sample on the sample stage was measured.
3. Scanning direction of the piezoelectric drive was measured against the sample from STM image.
4. Information obtained by procedure 1, 2 and 3 was combined to derive the angle of magnetic field against STM image

Figure A.2 shows the combined information. Blue allow which indicates the direction of magnetic field was drawn using information from procedure 1. Pink arrows are possible direction of $[2\bar{1}\bar{1}]$ direction of the sample on the sample stage. Black arrows are drawn based on information from procedure 3. The STM image obtained when the sample was in setting C is shown in Fig. A.3. The $[2\bar{1}\bar{1}]$ direction can be identified from the direction of the steps. Thus, the x and y scan direction is known to 183° and 93° from $[2\bar{1}\bar{1}]$ direction respectively. (Note that Figure A.2 is top view, while we see bottom view in the STM image.) In Fig. A.4, the schematic image of magnetic field direction against STM image (bottom view) extracted from Fig. A.2 is shown.

* The relative angle between the cryostat and the vacuum chamber is variable by rotating the cryostat.

** Exchange of piezoelectric drive (because of some trouble, for example,) requires reexamination of the scanning direction.

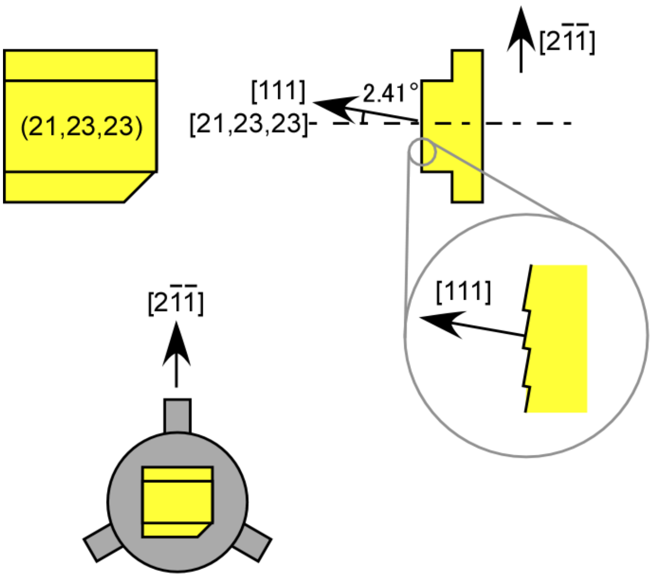

Figure A.1 The configuration of the sample on the sample holder.

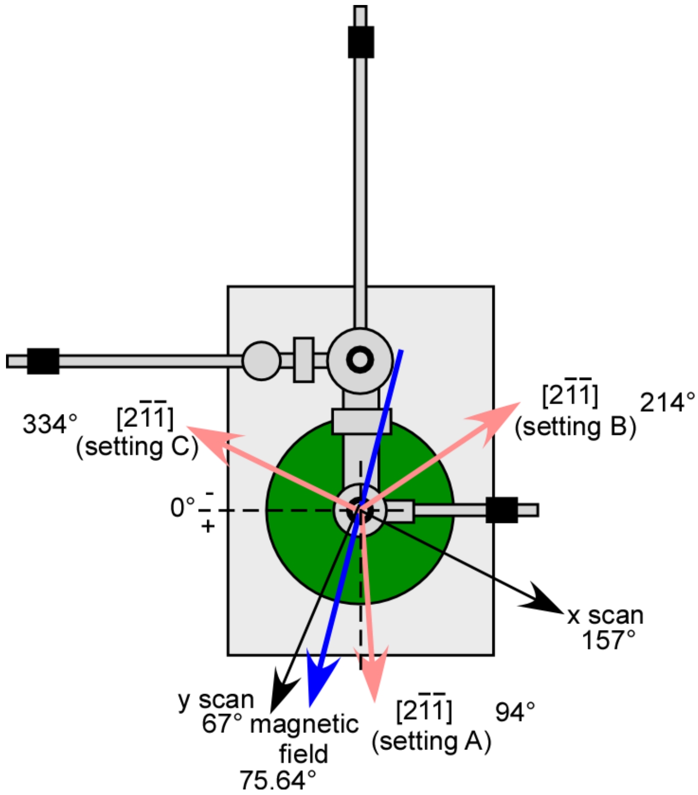

Figure A.2 Schematic image of the direction of magnetic field, x and y scan.

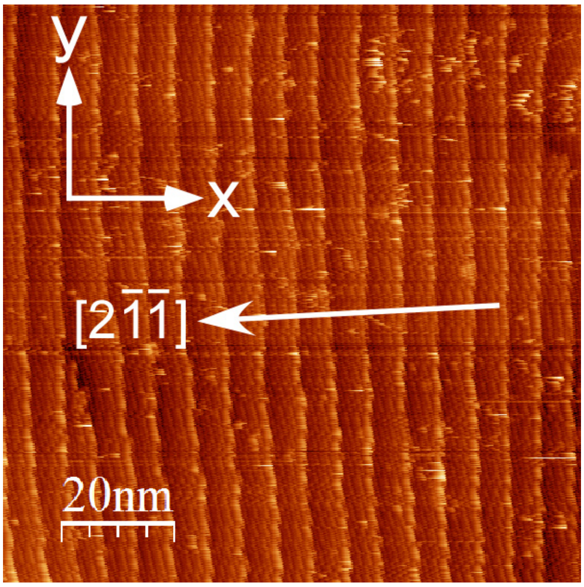

Figure A.3 STM image of the vicinal surface at setting C.

T = 3 K, V = −48 mV, I = 190 pA, 100 nm×100 nm

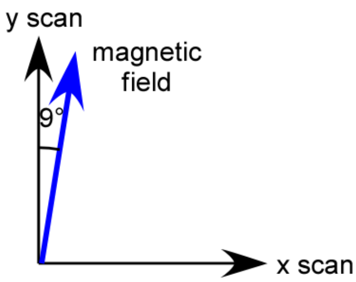

Figure A.4 Direction of magnetic field in the STM image.

Appendix B: STS spectra of dense FePc monolayer on Au(111)

Appendix B is not included in the online version because it includes unpublished data.

Acknowledgement

本研究を遂行するにあたりお世話になった方々にお礼申し上げます。まず、研究生活を共に過ごした東京大学大学院・新領域創成科学研究科・物質系専攻、川合・髙木研究室のメンバーにお礼申し上げます。川合眞紀教授には、この上ない研究環境をご用意いただき、また、日々の研究を暖かく見守っていただいたことに感謝いたします。髙木紀明准教授には、研究生活のあらゆる面でお世話になりました。聞き上手な高木先生のおかげで、つまらない疑問や悩み、アイディアも口に出すことができました。高木先生との会話は、研究を進める原動力になったと思います。ありがとうございました。塚原規志助教には、装置の扱い方から、トラブル時の対応まで、色々な事を教えていただきました。塚原さんとのディスカッションは、研究計画を立てる上でとても役に立ちました。お礼申し上げます。荒船竜一客員研究員には、HREELS 測定で装置を貸していただきました。また、論文の書き方、実験データの整理の仕方等、荒船さんから教わったことは数知れません。ありがとうございました。林俊良特任助教には、ミーティングや発表練習の際、いつも的確なご指摘やご質問をいただきました。また、研究や進路について悩んでいるとき、相談に乗って頂いたり、励ましたりしていただきました。ありがとうございます。白木将元助教には、東北大にお邪魔した際、光電子分光についてご指導いただいた他、色々な装置を紹介していただきました。ありがとうございます。上羽弘元特任教授が柏キャンパスに在籍された一年間は、私にとってとても刺激的な一年間でした。上羽先生が開いてくださった特別講義のおかげで、理論研究がどのような動機やアイディアに基づいて行われているかを体感することができました。柏に来てくださってありがとうございました。研究室の博士課程の先輩である本林健太さん、松永宗一郎さんは、在学中、素晴らしいリーダーシップで学生をまとめてくださいました。また、山本真祐子さん、能登健一さん、八百篤史さん、黒田彩夏さん、酒井真利さんには、柏での生活の仕方を教えていただいたり、長丁場の実験のコツを教えていただいたりしました。先輩方のおかげで、楽しく研究生活のスタートを切る事ができました。ありがとうございます。同期の平岡諒一さん、福嶋徹さん、水澤岳さん、野村周平さん、伊藤研の高橋祥子さんは一番身近な研究仲間であると同時に、目標でもありました。皆様のおかげで楽しい研究生活を送れました。ありがとうございました。一学年上の博士課程の先

輩であった梁賢眞さんからは、博士論文執筆にあたり、ご自身の用いたツールなどを教えていただきました。感謝いたします。後輩の皆様からも、研究に向かう姿勢、課題解決のためのアプローチの方法などに関して、たくさんの刺激を受けました。ありがとうございました。研究室秘書の和泉嘉枝さんには、事務手続き全般を手伝っていただきました。快適な博士生活が遅れたのは和泉さんのおかげです。ありがとうございました。

理化学研究所、表面科学研究室の皆様にもお礼申し上げます。金有洙研究員、山田太郎元研究員、清水智子元研究員、今田裕研究員には、東大川合研、理研表面科学研究室で合同ミーティングを行っていた際、発表の仕方や表現などについてご指導いただきました。感謝いたします。南谷英美元研究員には、近藤効果を研究する理論家として、基本的な疑問点に応えて頂いたり、実験結果の解釈について議論させていただいたり、VASP の使用法をご教授いただいたりと非常にお世話になりました。お礼申し上げます。

最後に、研究生活を支え、応援してくださった父母、祖父母、妹に感謝いたします。

2015 年 1 月

太田 奈緒香

Bibliography

Publications

1. N. Tsukahara, S. Shiraki, S. Itou, N. Ohta, N. Takagi, and M. Kawai
Evolution of Kondo Resonance from a Single Impurity Molecule to the Two-Dimensional Lattice, Phys. Rev. Lett. **106**, 187201 (2011).

2. N. Ohta, R. Arafune, N. Tsukahara, M. Kawai, and N. Takagi
Enhancement of Inelastic Electron Tunneling Conductance Caused by Electronic Decoupling in Iron Phthalocyanine Bilayer on Ag(111), J. Phys. Chem. C **117**, 21832 (2013).

3. N. Ohta, R. Arafune, N. Tsukahara, N. Takagi, and M. Kawai
Adsorbed states of iron(II) phthalocyanine on Ag(111) studied by high-resolution electron energy loss spectroscopy, Surf. Interface Anal. **46**, 1253 (2014).

Presentations (international conferences)

1. N. Ohta, R. Arafune, N. Tsukahara, N. Takagi, and M. Kawai
Inelastic electron tunneling through iron phthalocyanine molecules on Ag(111), 12th International Conference on Electron Spectroscopy and Structure, Saint-Malo, France, September 2012. (poster)

2. N. Ohta, R. Arafune, N. Tsukahara, N. Takagi, and M. Kawai
Effects of the local environment on the inelastic electron tunneling spectra of iron(II) phthalocyanine molecules on Ag(111), 14th International Conference on Vibrations At Surfaces. Hyogo, Japan, September 2012. (poster)

3. N. Ohta, K. Shindo, M. Furushima, N. Tsukahara, N. Takagi, and M. Kawai
Adsorption structure of iron phthalocyanine bilayer on silver surfaces, 12th International Conference on Atomically Controlled Surfaces, Interfaces and Nanostructures in conjunction with 21st International Colloquium on Scanning Probe Microscopy, Ibaraki, Japan, November 2013. (poster)

4. N. Ohta, R. Arafune, N. Tsukahara, N. Takagi, and M. Kawai
Enhancement of inelastic electron conductance changes driven by reduced molecule-substrate interaction in iron phthalocyanine bilayer on Ag(111), 9th

International Symposium on Atomic Level Characterizations for New materials and Devices' 13 , Hawaii, USA, December 2013. (poster)

5. <u>N. Ohta</u>, R. Arafune, N. Tsukahara, N. Takagi, and M. Kawai

Large conductance change in inelastic electron tunneling spectra of iron phthalocyanine / Ag(111) , Gorodon Research Conference (Vibrational Spectroscopy), Maine, USA, August 2014. (poster)

6. N. Ohta, N. Tsukahara, N. Takagi, and M. Kawai

Magnetic response of scanning tunneling spectra of a Kondo lattice: iron phthalocyanine molecular lattice on Au(111), The 7th International Symposium on Surface Science, Shimane, Japan, November 2014. (poster)

Presentations (domestic conferences)_

1. 太田奈緒香, 塚原規志, 髙木紀明, 川合眞紀

表面２次元近藤格子の走査トンネル分光スペクトル：磁場依存と空間分布, 日本物理学会第 68 回年次大会, 広島, 2013 年 3 月.（口頭）

2. 太田奈緒香, 進藤一樹, 古島弥来, 塚原規志, 髙木紀明, 川合眞紀

銀表面に２層吸着した鉄フタロシアニン分子の吸着構造とその面方向依存, 日本物理学会 2013 年秋季大会, 徳島, 2013 年 9 月.（口頭）

3. 太田奈緒香, 荒船竜一, 塚原規志, 川合眞紀, 髙木紀明

分子振動励起による巨大コンダクタンス変化, 文部科学省研究費補助金「新学術領域域研究」分子アーキテクトニクス：単一分子の組織化と新機能創成 第 4 回分子アーキテクトニクス研究会, 東京, 2014 年 3 月.（ポスター）

4. 太田奈緒香, 塚原規志, 髙木紀明, 川合眞紀

表面近藤格子、Au(111)表面吸着鉄フタロシアニン格子の異方的磁気応答, 日本物理学会 2014 年秋季大会, 愛知, 2014 年 9 月.（口頭）